ADVANCED OPTICAL MATERIALS
www.advopticalmat.de

Enhanced Excitonic Nature of $MAPbBr_3$ Nanocrystals in Nanoporous GaN

Xinyu Bai, Simon M. Fairclough, Linjie Dai, Maruf Sarkar, Peter H. Griffin, Abhiram Gundimeda, Yuqi Sun, Neil C. Greenham, M. Ibrahim Dar, Rachel A. Oliver,* and Richard H. Friend**

Blue gallium nitride (GaN) light-emitting diodes (LEDs), combined with red/green fluorescent converters, have broad potential for display applications. Metal halide perovskites now show excellent luminescence properties and may be suitable as light converters. Here a simple solution-processed method is reported to prepare a methylammonium lead bromide ($MAPbBr_3$) nanoporous GaN composite. Fast (within 2 ps) energy transfer is demonstrated from photoexcited nanoporous GaN to encapsulate $MAPbBr_3$ nanocrystals, as observed by transient absorption spectroscopy. The spatial confinement of the perovskite within the nanoporous GaN is shown to increase the perovskite radiative recombination rate. These results offer guidelines for developing high-performance perovskite/nanoporous GaN optoelectronics.

1. Introduction

Gallium nitride (GaN) possesses exceptional optical and electrical properties, including good electrical and thermal conductivity, chemical stability, and high decomposition temperature. It has enabled light-emitting diodes (LEDs) with high emission efficiency and long operational lifetime.[1–4] With the development in the porosification of epitaxial GaN via doping-selective electrochemical etching,[5,6] porous GaN offers an opportunity to produce composite materials through the infiltration of pores and thus broaden its application in numerous electronic and optoelectronic devices,[7–12] including color-converting micro-light emitting diodes (Micro-LEDs).[13–18] GaN-based blue micro-LEDs combined with red and green light converters, such as organic semiconductors[13–15] and inorganic quantum dots,[16–18] have been fabricated and show promise for full-color displays. However, the πconjugated organic light converters often suffer from broad emission spectra.[13–15] Therefore, they cannot satisfy demands for spectrally purest color conversion required to get the purest color gamut. Meanwhile, the preparation process of inorganic quantum dot light converters is complex and expensive.[16–18] On the other hand, in recent years, lead halide perovskites have become an attractive class of light conversion materials since they show high absorption in the UV/Blue region,[19] high defect tolerance,[20,21] color tunability,[22–24] narrow-band emission,[23,25] low-temperature synthesis process,[26] and affordability. However, for 3D perovskite thin films, such as methylammonium lead bromide perovskite ($MAPbBr_3$), the dominant charge carriers are free electrons and holes at room temperature due to low exciton binding energy.[27] As a result, the achievable photoluminescence quantum efficiency (PLQE) of pristine $MAPbBr_3$ thin film is relatively low (<1%–10%).[24,27–30] To overcome this limitation, nanoporous matrices, such as silica,[31] alumina,[32,33] and titania[34], were used to confine perovskite growth into nanocrystals. This confinement can enhance the radiative recombination and boost the PLQE of perovskite. There are reports of infiltration of perovskite material into nanoporous GaN.[7,35] It has been demonstrated that the nanoporous GaN structure could preserve infiltrated perovskite photoluminescence for up to one year and enhance the photoluminescence of perovskite in nanopores.[35] However, the mechanisms behind the optimization of photoluminescence have yet to be studied. Here, we investigate the composite's morphology and the charge carrier dynamics in the heterostructure to offer guidelines for developing high-performance perovskite/nanoporous GaN optoelectronics in the future.

2. Results and Discussion

2.1. Preparation and Structural Characterizations of $MAPbBr_3$/Nanoporous GaN Composite

Nanoporous GaN pseudo-substrates (Figure S1, Supporting Information) were prepared via electrochemical etching of Si-doped

X. Bai, L. Dai, Y. Sun, N. C. Greenham, M. I. Dar, R. H. Friend
Cavendish Laboratory
University of Cambridge
Cambridge CB3 0HE, UK
E-mail: id338@cam.ac.uk; rhf10@cam.ac.uk

S. M. Fairclough, M. Sarkar, P. H. Griffin, A. Gundimeda, R. A. Oliver
Department of Materials Science & Metallurgy
University of Cambridge
Cambridge CB3 0FS, UK
E-mail: rao28@cam.ac.uk

The ORCID identification number(s) for the author(s) of this article can be found under https://doi.org/10.1002/adom.202400221

© 2024 The Author(s). Advanced Optical Materials published by Wiley-VCH GmbH. This is an open access article under the terms of the Creative Commons Attribution License, which permits use, distribution and reproduction in any medium, provided the original work is properly cited.

DOI: 10.1002/adom.202400221

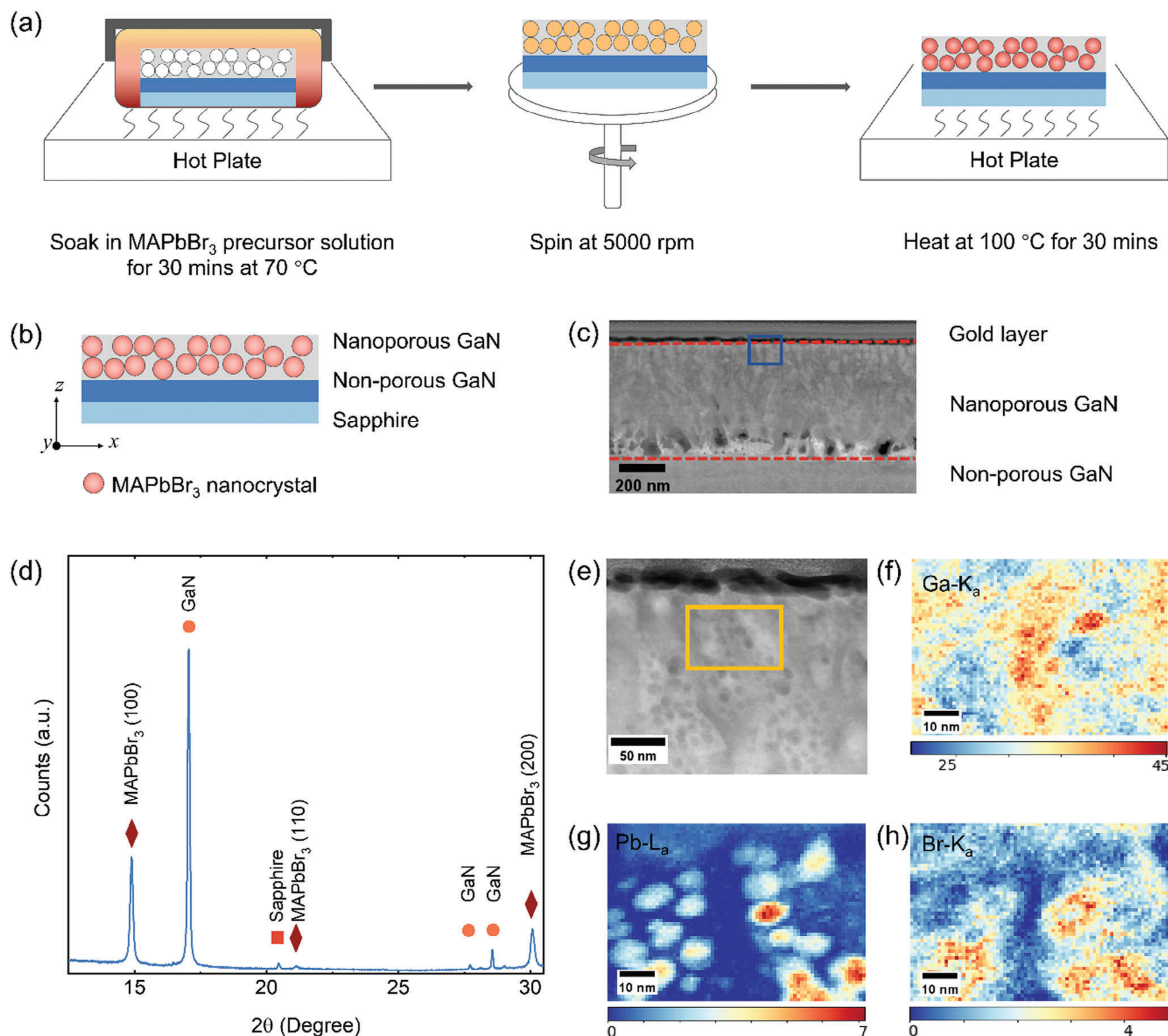

Figure 1. $MAPbBr_3$/nanoporous GaN preparation and characterization. a) Schematic diagram of $MAPbBr_3$/nanoporous GaN composite preparation process. Pristine nanoporous GaN (white circles represent pores) is soaked in 70 °C precursor solution on the hot plate for 30 min, followed by spinning at 5000 rpm (yellow circles represent precursor solution in pores) and annealing at 100 °C (Orange circles represent perovskite nanocrystals in pores); b) schematic diagram of $MAPbBr_3$/nanoporous GaN sample's cross-section; c) cross-sectional bright field-STEM of the $MAPbBr_3$/nanoporous GaN sample, scale bar: 200 nm; d) X-ray diffraction (XRD) pattern of $MAPbBr_3$/nanoporous GaN, red labeled peaks are (100), (110), and (200) planes of $MAPbBr_3$; e) zoomed-in cross-sectional bright fieldSTEM in the blue square in (c), scale bar: 50 nm; EDX elemental maps of the yellow square area (125 nm × 75 nm) in (e); f) gallium (Ga-K_a), g) lead (PbL_a), and h) bromine (BrK_a), show the intensity for the elements, scale bar: 10 nm, color bar: atomic percentage (%). The thickness of the STEM sample is less than 100 nm.

GaN epitaxial layers on sapphire substrates with 0.25 M aqueous oxalic acid as the electrolyte at 8 V.[6,35] The as-etched nanoporous GaN wafers were ultrasonically cleaned in acetone and then isopropanol for 15 min, respectively. The cleaned substrates were baked in an oven at 500 °C for three hours to evaporate moisture inside the nanopores. After cooling to room temperature, these dry GaN substrates were given an oxygen plasma treatment at a power of 50 W for 15 min, which decorates the surface with hydrophilic groups to assist wetting. The nanoporous GaN substrates were then transferred into a nitrogen-filled glovebox. A 1.0 M $MAPbBr_3$ precursor solution was prepared by dissolving 1 mmol $PbBr_2$ and 1 mmol MABr in 1 mL dimethylformamide (DMF): Dimethyl sulfoxide (DMSO) = 9:1 solvent. A ≈1 cm^2 GaN substrate was soaked in 1 mL 1.0 M $MAPbBr_3$ precursor solution for 30 min at 70 °C. Subsequently, the perovskite precursor infiltrated nanoporous GaN substrate was spun at 5000 rpm to remove the excess solution at the surface. The sample was annealed at 100 °C for 30 min to crystallize the $MAPbBr_3$ inside the nanopores (**Figure** 1a). The sample surface was further cleaned with isopropanol-soaked clean room tissue to remove ex-

© 2024 The Author(s). Advanced Optical Materials published by Wiley-VCH GmbH

cess perovskite. Samples for transient characterization were encapsulated in the nitrogen-filled glovebox to reduce perovskite degradation when exposed to air and moisture.

We examine the $MAPbBr_3$/nanoporous GaN composite with X-ray diffraction (XRD). Figure 1d shows the XRD pattern of the $MAPbBr_3$/nanoporous GaN composite. The XRD peaks at 14.88° and 30.07° are the (100) and (200) planes of the Pm3m cubic phase $MAPbBr_3$ perovskite.[36,37] Other XRD peaks are assigned to the pristine nanoporous GaN on the sapphire substrate (Figure S2, Supporting Information). The XRD measurement suggests the successful synthesis of phase pure $MAPbBr_3$ with the one-step deposition method. To establish the structure of the infiltrated $MAPbBr_3$, we have carried out cross-sectional scanning transmission electron microscopy (STEM) of the $MAPbBr_3$/nanoporous GaN composite. The cross-sectional bright-field (BF) STEM in Figure 1c clearly reveals the non-porous GaN layer, the nanoporous GaN layer above (≈500 nm), and a ≈20 nm thick capping gold layer–required for the focused ion beam (FIB) sample preparation process. The electrochemical etching of the Si-doped GaN creates an open and connected pore morphology (lateral pore sizes ranging from 15 to 50 nm). The porous network has irregular morphology with various longitudinal length scales (20 to 200 nm). Nanoparticles with diameters ranging from 7 to 15 nm are resolved inside the nanopores (Figure 1e). The nanoparticles were seen over almost 500 nm within the porous GaN. Energy-dispersive X-ray spectroscopy (EDX) elemental maps from the top region (≈50 nm to the surface) marked by a yellow box in Figure 1e (which itself relates to the blue box in Figure 1c) are displayed in Figure 1f–h. The lead (Pb) (Figure 1g) and bromine (Br) (Figure 1h) signals are observed in regions where a weak Ga signal is seen (Figure 1f), i.e., the position of nanopores. Additionally, strong Pb and Br signal regions match the nanoparticles' positions in Figure 1e (Figure S3, Supporting Information).

We calculated the effective thickness of perovskite from the steady-state absorption spectrum (**Figure 2**a). The absorption coefficient of $MAPbBr_3$ is $\alpha = 4.1 \times 10^4$ cm^{-1} at 500 nm (2.48 eV) (Figure 2b) (Figure S4, Supporting Information). The absorbance of $MAPbBr_3$/nanoporous GaN at 500 nm is $A = 0.184$ (Figure 2a). According to the Beer–Lambert Law.[38] ($l = 2.303^{*}A/\alpha$, l is the sample thickness, A is the absorbance, and α is the absorption coefficient), the effective thickness of the perovskite layer is ≈100 nm. Cross-sectional SEM measurement on a similar nanoporous GaN sample suggests a porosity of ≈30%–40%.[39] According to this observation, more than 50% of the pores have been filled with perovskite nanocrystals.

2.2. Energy Transfer Between GaN and Perovskite

We have tracked the photogenerated carrier dynamics in these $MAPbBr_3$/Nanoporous GaN composite with time-resolved photoluminescence (TRPL) spectroscopy and transient absorption (TA) spectroscopy. When the composite is excited above the GaN absorption edge at 350 nm, photoluminescence (PL) peaks of both a broad yellow band (centered at 569 nm) due to emission from the GaN (its origin is discussed later) (Figure S5, Supporting Information) and $MAPbBr_3$ (centered at 530 nm) are observed (Figure 2c), green line). With photoexcitation at 400 nm, at which only $MAPbBr_3$ is excited, the yellow band emission from GaN disappears, and only the perovskite PL peak at 530 nm is detected (Figure 2c), blue line). As reported in the literature,[40] GaN and $MAPbBr_3$ form a Type I heterojunction, and energy transfer from GaN to the perovskite is expected. We have used TA to investigate the charge carrier kinetics in the composite. We excite the $MAPbBr_3$/nanoporous GaN at either 340 or 400 nm from the nanoporous GaN side. Both pump intensities are kept low (11 µJ cm^{-2} per pulse at 340 nm and 14 µJ cm^{-2} per pulse at 400 nm) to avoid Auger recombination. Figure 2d shows a TA pseudocolor map of $MAPbBr_3$/nanoporous GaN excited at 340 nm, and both GaN and $MAPbBr_3$ are excited. Two positive signals, due to ground state bleach (GSB), are observed at ≈375 nm (GaN) and 525 nm (perovskite). The nanoporous GaN does not absorb the 400 nm laser. (Figure S6, Supporting Information) When the composite is excited at 400 nm, only the GSB of $MAPbBr_3$ is probed, as seen in Figure 2e. Time traces at the GSB of $MAPbBr_3$ under 340 and 400 nm pumps are shown in Figure 2g. When the sample is excited at 400 nm (blue line), the perovskite GSB builds up instantly. In contrast, when both GaN and $MAPbBr_3$ are excited at 340 nm, the perovskite GSB kinetic rises more slowly and reaches its maximum at 1.5 ps after excitation (green line). We attribute this slower rise to energy transfer from the nanoporous GaN.

Figure 2f shows the TA pseudocolor map of the nanoporous GaN excited at 340 nm at 11 µJ cm^{-2} per pulse. We extracted the time traces at the GSB of GaN under 340 nm pump in the presence and absence of perovskite from Figure 2d–f and shown in Figure 2h. GaN's GSB of $MAPbBr_3$/nanoporous GaN decays faster than when the perovskite is absent. It suggests that $MAPbBr_3$ nanocrystals are able to quench the excitation states of GaN in the first 1 ns after excitation. In order to see how long this transfer process lasts, we took the TRPL at 360 nm of the pristine nanoporous GaN and $MAPbBr_3$/Nanoporous GaN when photoexcited at 255 nm (Figure S7, Supporting Information). With the presence of $MAPbBr_3$, GaN's emission decays faster in the first 10 ns after photoexcitation than when the perovskite is absent. Beyond 10 ns, the PL decay of GaN's PL shows the same trend with and without perovskite. These phenomena suggest that the energy transfer from nanoporous GaN terminates by 10 ns after excitation. We note that the cross-section STEM (Figure 1e) shows some perovskite nanocrystals sitting in the middle of the nanopores. Such nanocrystals may not be within the energy transfer distance. Therefore, limited by the energy transfer distance, not all perovskite nanocrystals are able to harvest the energy from GaN. As a consequence, the energy transfer process will end when the perovskite nanocrystals within the transfer distance are all excited, shown as this short-term energy transfer process.

We estimated the proportion of energy that can transfer from the nanoporous GaN to $MAPbBr_3$. The absorbance of the perovskite at 340 nm is 0.59, see Figure 2a. Since the total absorbance at 340 nm for $MAPbBr_3$ and nanoporous GaN is 2.6, ≈77% of photons are absorbed by GaN, and $MAPbBr_3$ absorbs 23%. Therefore, if no energy transfer happened, the GSB intensity should be 25% of the GSB when excited at 400 nm (Figure 2f), black dashed line) at the same excitation fluence. Based on the absorbance percentage at 340 nm for $MAPbBr_3$/nanoporous GaN, we estimated the GSB intensity if all the energy harvested by the

© 2024 The Author(s). Advanced Optical Materials published by Wiley-VCH GmbH

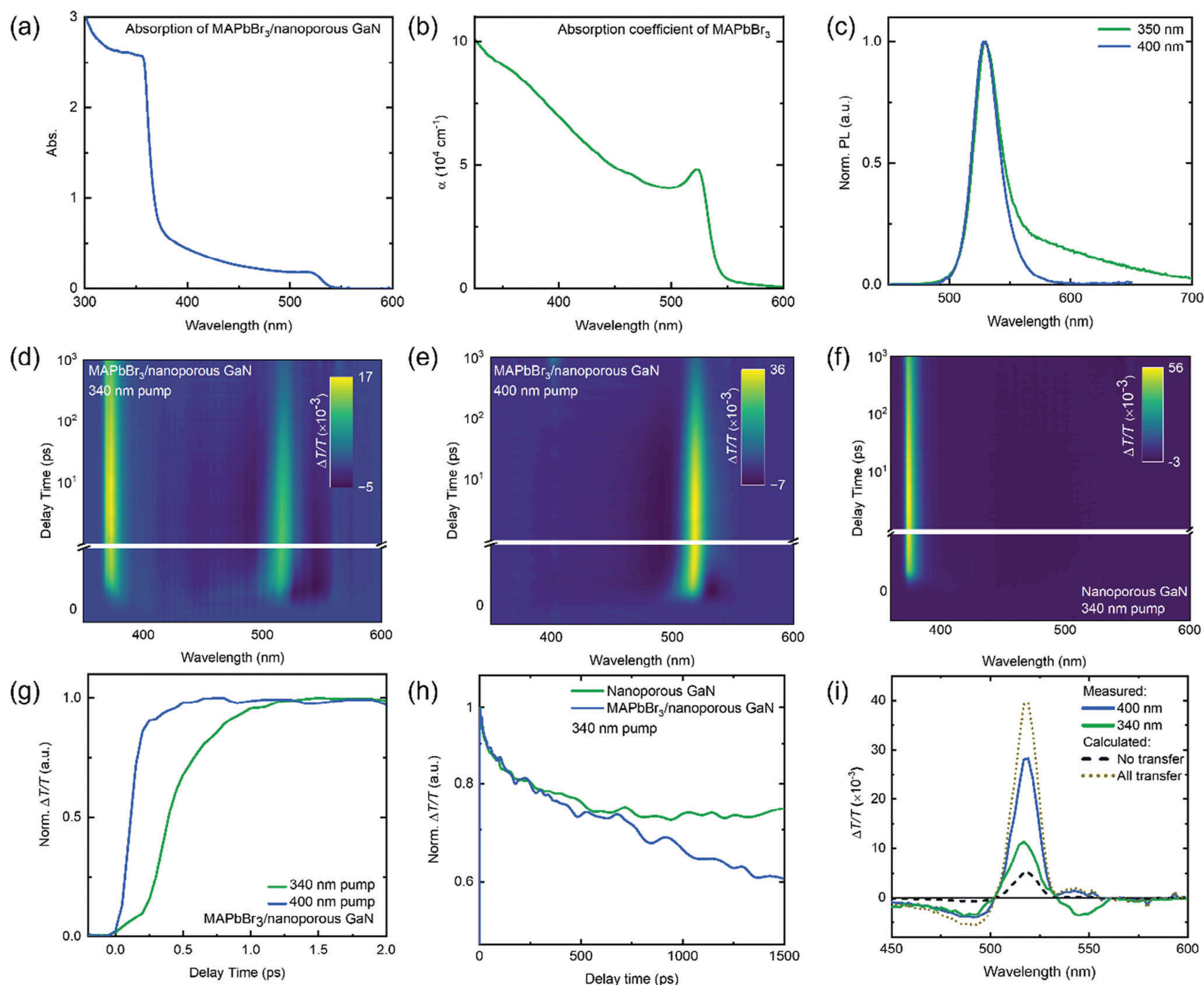

Figure 2. Energy transfer between $MAPbBr_3$ and GaN. a) Steady-state absorption spectrum of $MAPbBr_3$/nanoporous GaN. b) The absorption coefficient of $MAPbBr_3$ thin film. c) Normalized steady-state photoluminescence spectra of $MAPbBr_3$/nanoporous GaN, excited at 350 nm (Green line) and 400 nm (Blue line). d) Transient absorption pseudocolor map of $MAPbBr_3$/nanoporous GaN excited at 340 nm. The y-axis is linear up to 1 ps and logarithmic thereafter. e) Transient absorption pseudocolor map of $MAPbBr_3$/nanoporous GaN excited at 400 nm (exciting $MAPbBr_3$ only). The y-axis is linear up to 1 ps and logarithmic thereafter. f) Transient absorption pseudocolor map of nanoporous GaN excited at 340 nm. The y-axis is linear up to 1 ps and logarithmic thereafter. g) The normalized kinetics for the ground state bleach of $MAPbBr_3$ when $MAPbBr_3$/nanoporous GaN was under a 340 nm pump (Green line) and a 400 nm pump (Blue line). Kinetics are normalized to the maximum $\Delta T/T$. Kinetics are extracted from (d) and (e) respectively. h) The normalized kinetics for the ground state bleach of GaN when the pristine nanoporous GaN (Green line) and $MAPbBr_3$/nanoporous GaN (Blue line) were under a 340 nm pump. Kinetics are extracted from (d) and (f), respectively. The y-axis is logarithmic. i) The transient absorption spectra when the GSB reaches its maximum under the photoexcitation at 340 nm (Green line) and 400 nm (Blue line). The spectra are extracted from (d) and (e), respectively. The black dashed line is the calculated spectra if no energy transfer occurs at 340 nm excitation. The yellow dot line is the calculated spectra if all energy harvested by GaN would transfer to perovskite at 340 nm excitation. The initial ($t = 0$) average fluence of the 340 nm pump is 11 μJ cm^{-2} per pulse over the illuminated area. The initial ($t = 0$) average fluence of the 400 nm pump is 14 μJ cm^{-2} per pulse over the illuminated area.

GaN were transferred to $MAPbBr_3$, which is 1.1 times the perovskite's GSB when excited at 400 nm, shown as the yellow dot line in Figure 2i. We observe a $MAPbBr_3$ GSB signal for pumping at 340 nm (Figure 2i), green line), whose area is 1.8 times the calculated GSB area when no transfer happens. Putting these observations together, we estimated that ≈25% of the energy harvested by GaN will transfer to $MAPbBr_3$ nanocrystals.

We also notice that when only $MAPbBr_3$ is photoexcited, only PL of perovskite can be observed while the yellow band emission from GaN is absent (Figure 2d). The origin of the yellow band emission is under debate in the nitride community. Most investigations suggest that the emission is related to point defects and involves deep states in the bandgap. For example, one potential origin of the yellow band is emission from gallium vacancy-related defects,[41] leading to a transition between the conduction band/shallow donor and a deep acceptor state.[42] The absence of yellow band emission when the composite is excited below the GaN bandgap suggests that the yellow band defect levels

© 2024 The Author(s). Advanced Optical Materials published by Wiley-VCH GmbH

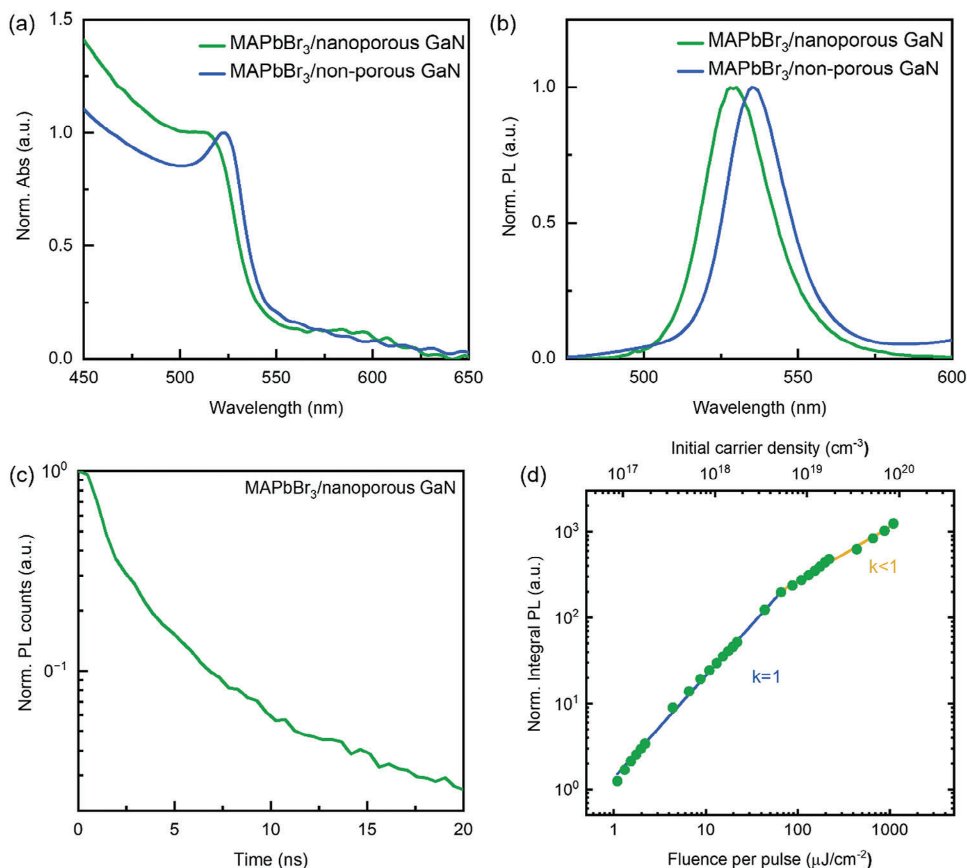

Figure 3. Charge carrier dynamics of $MAPbBr_3$/GaN composites a) Normalized steady-state absorption spectra of $MAPbBr_3$/nanoporous GaN (Green line) and $MAPbBr_3$/non-porous GaN (Blue line). b) Normalized photoluminescence spectra of $MAPbBr_3$/nanoporous GaN (Green line) and $MAPbBr_3$/non-porous GaN (Blue line). Samples were excited at 400 nm. c) Transient PL of $MAPbBr_3$/nanoporous GaN under 407 nm laser excitation at 0.07 μJ cm^{-2} per pulse. The kinetic was taken at the PL peak of $MAPbBr_3$. The *y*-axis is logarithmic. d) Fluence-dependent integral PL of $MAPbBr_3$ for $MAPbBr_3$/nanoporous GaN when the sample was excited at 400 nm from 1 to 1000 μJ cm^{-2} over the illuminated area.

in GaN cannot harvest the radiative energy from perovskite, and no energy transfer from perovskite to GaN's defect levels is observed.

The nanoporous structure of GaN is critical in achieving energy transfer from GaN to perovskite. We notice that the GSB rising kinetics are the same for the 340 nm pump and 400 nm pump conditions for $MAPbBr_3$/non-porous GaN heterojunction, with the absence of a slow GSB build-up process. No energy transfer in a $MAPbBr_3$/non-porous GaN heterojunction is observed (Figure S8, Supporting Information). We suppose that the nanoporous structure results in a much larger interfacial area between GaN and perovskite than at the perovskite/non-porous GaN heterojunction, which benefits the energy transfer process shown in Figure 2g. According to the cross-section STEM in Figure 1e, the lateral pore length of the nanoporous GaN can be as short as 15 nm. Therefore, the majority of $MAPbBr_3$ nanocrystals in pores sit adjacent to the GaN surface, while the thickness of $MAPbBr_3$ thin film means that a much smaller proportion of the perovskite experiences any energy transfer when it is present at the non-porous GaN surface. As a consequence, more perovskite in the porous GaN could harvest the energy from the photoexcited GaN due to the much shorter energy transfer distance.

2.3. Confinement Effect of Nanoporous GaN on Perovskite Nanocrystals

We have studied the influence of the nanoporous structure of GaN on the charge carrier recombination behavior in $MAPbBr_3$. **Figure 3a** presents the $MAPbBr_3$ absorption onset of $MAPbBr_3$/nanoporous GaN (Green line) and $MAPbBr_3$/non-porous GaN (Blue line). The direct bandgap of perovskite derived from the Tauc plot (Figure S9, Supporting Information) is 2.31 eV for the $MAPbBr_3$/non-porous GaN sample and 2.33 eV for the $MAPbBr_3$/nanoporous GaN sample, so only a 0.2 meV blueshift in band edge appears when perovskite is in the nanoporous GaN matrix. Consistent with the steady-state UV–vis absorption result, the perovskite PL peak of the $MAPbBr_3$/non-porous GaN sample is 540 nm, and that of the $MAPbBr_3$/nanoporous GaN sample is 535 nm (Figure 3b). No significant blueshift in perovskite PL spectra is observed. The cross-section STEM shows that some perovskite nanocrystal sizes could reach 30 nm (Figure 1e), while the Bohr radius of $MAPbBr_3$ is 4.7 nm.[43] Therefore, the crystal size of the $MAPbBr_3$ inside nanopores is too large to achieve significant quantum confinement. Consequently, no broadening in bandgap is observed in both steady-state absorption and PL measurement.

© 2024 The Author(s). Advanced Optical Materials published by Wiley-VCH GmbH

Table 1. Calculated recombination constants from the recombination rates measured with TCSPC in Figure 3c and Figure S10 (Supporting Information). The calculation method is demonstrated in Note S1 (Supporting Information). τ_{PL} is the average PL lifetime extracted from the TCSPC, τ_{rad} is the radiative recombination lifetime, and $\tau_{non\text{-}rad}$ is the non-radiative recombination lifetime k_{PL} is the average recombination rate, $k_{non\text{-}rad}$ is the non-radiative recombination rate and k_{rad} is the radiative recombination rate.

Sample [units]	τ_{PL} ns	k_{PL} s^{-1}	τ_{rad} Ns	k_{rad} s^{-1}	$\tau_{non\text{-}rad}$ Ns	$k_{non\text{-}rad}$ S^{-1}
$MAPbBr_3$/Nanoporous GaN	28	3.55×10^7	220	4.61×10^6	32	3.09×10^7
$MAPbBr_3$/non-porous GaN	123	8.12×10^6	4100	2.44×10^5	127	7.88×10^6

The PLQE with 405 nm excitation.[44] for $MAPbBr_3$ thin film is only 3%, falling within the range reported for $MAPbBr_3$ thin films,[24,27–30] while the PLQE for perovskite PL of the $MAPbBr_3$/nanoporous GaN composite reaches 13%. To investigate the charge carrier recombination dynamics for the infiltrated perovskite, we measure the transient PL with time-correlated single-photon counting (TCSPC) at the perovskite's emission peak of $MAPbBr_3$/nanoporous GaN with that of the $MAPbBr_3$/non-porous GaN in Figure 3c (Figure S10, Supporting Information) when excited at 407 nm. The PL decays significantly faster for perovskite inside the nanopores. Meanwhile, the GSB for $MAPbBr_3$ in $MAPbBr_3$/nanoporous GaN also decays faster than that of the $MAPbBr_3$/non-porous GaN under a 400 nm pump (Figure S11, Supporting Information). As discussed before, no energy transfer from perovskite to GaN's defect level is observed from TA measurement when only $MAPbBr_3$ is excited. Therefore, we rule out the possibility that such an energy transfer process leads to faster decay in transient PL and TA measurement.

We extract the average PL lifetime from the transient PL result in Figure 3c (Figure S10 and Note S2, Supporting Information). By combining the average PL lifetime and the PLQE, we calculated the radiative recombination rate and non-radiative recombination rate based on equations:

$$k_{PL} = k_{non-rad} + k_{rad} \tag{1}$$

$$PLQE = \frac{k_{rad}}{k_{non-rad} + k_{rad}} \tag{2}$$

$$k = \frac{1}{\tau} \tag{3}$$

where k_{PL} is the average recombination rate, $k_{non\text{-}rad}$ is the non-radiative recombination rate, and k_{rad} is the radiative recombination rate. The recombination rate (k) equals the reciprocal of a lifetime (τ). The calculated results are listed in **Table 1**. We know from the calculation that both radiative and non-radiative recombination rates increase when $MAPbBr_3$ is confined in the nanoporous GaN compared to perovskite thin film at the non-porous GaN surface. The faster non-radiative recombination in the $MAPbBr_3$/nanoporous GaN than that of $MAPbBr_3$/nonporous GaN (≈4 times faster) can potentially be attributed to the increased surface area and hence the density of trap states due to the smaller crystal size.

On the other hand, perovskite nanocrystals inside the nanoporous GaN structure show a much faster radiative recombination rate compared to the bulk perovskite thin film (≈20 times faster). Therefore, the overall PLQE of the $MAPbBr_3$/nanoporous GaN sample is still much higher than that of the $MAPbBr_3$/non-porous GaN sample. We measured the fluence-dependent PL to test our hypothesis further. When samples are excited at 400 nm, the integrated PL intensity (I) increases linearly with the pump fluence (P) below 100 μJ cm^{-2} per pulse ($I \sim P^1$) (Figure 3d). Schmidt et al. suggested that the integrated PL intensity I is proportional to P^K, where P is the excitation fluence. The exponent K is related to the dominant radiative recombination mechanism. When K is close to 1, it suggests a monomolecular recombination process dominates radiative recombination. When K is ≈2, it suggests a bimolecular recombination process dominates.[45] As shown in Figure 3d, $K = 1$ suggests the radiative recombination involves single electron–hole pairs for $MAPbBr_3$/nanoporous GaN. In contrast, the integrated PL intensity of perovskite thin film on the non-porous GaN increases quadratically with the pump fluence ($I \sim P^2$) (Figure S12, Supporting Information), indicating a dominant bimolecular recombination process. It has also been reported that the dominant radiative recombination process in $MAPbBr_3$ thin film at room temperature is the free charge carrier recombination due to the low exciton binding energy of $MAPbBr_3$.[27] The different behavior of perovskite in nanopores results from the localization of charge carriers in $MAPbBr_3$ nanocrystals inside nanoporous scaffolds. The size reduction spatially confines charge carriers in nanocrystals and enhances their localization. Therefore, the nanoporous GaN matrix enhances electron–hole interaction in perovskite nanocrystals via spatial confinement and increases exciton binding energy.

3. Conclusion

In conclusion, we demonstrate the energy transfer process from the nanoporous GaN to infiltrated $MAPbBr_3$ in the pores and the vital role of the porous structure in energy transfer. We note that the electron–hole interaction in perovskite is enhanced due to the spatial confinement, leading to a more efficient radiative recombination process, which is beneficial for achieving efficient light conversion in micro-LED displays. Our work provides a first step toward understanding the photophysical properties of the perovskite/nanoporous GaN heterostructure, and we demonstrate the potential for future application in color-converting micro-LEDs.

4. Experimental Section

Materials and Methods: Chemicals: Lead bromide ($PbBr_2$, 99.9999%), methylammonium bromide (MABr, 98%), acetone (99.9%), isopropyl alcohol (IPA, 99.9%), dimethylformamide (DMF, ≥ 99.9%), and Dimethyl sulfoxide (DMSO, ≥ 99.9%); purchased from the Sigma–Aldrich. These chemicals were utilized without further purification.

GaN Sample Preparation: The GaN samples were grown on sapphire by metal-organic vapor phase epitaxy. Growth commenced with a 4.4 μm thick low dislocation density GaN film on sapphire. This material was not intentionally doped (NID). This NID template was overgrowth with 500 nm of Si-doped GaN (≈10^{19} cm^{-3}). Nanoporous GaN pseudo-substrates were prepared via electrochemical etching of Si-doped GaN epi-

© 2024 The Author(s). Advanced Optical Materials published by Wiley-VCH GmbH

taxial layers on sapphire substrates with 0.25 M aqueous oxalic acid as the electrolyte at 8 V.[6,35]

$MAPbBr_3$/Non-Porous GaN Sample Preparation: A bi-layer $MAPbBr_3$/non-porous GaN sample was used as a reference in the subsequent investigation to compare with the $MAPbBr_3$/nanoporous GaN structure. Non-porous GaN wafers were ultrasonically cleaned in acetone and isopropanol for 15 min, respectively. Dry GaN substrates were subjected to oxygen plasma treatment at a power of 50 W for 15 min to decorate the surface with hydrophilic groups for optimal wetting. A 1.0 M $MAPbBr_3$ precursor solution was prepared by dissolving 1 mmol $PbBr_2$ and 1 mmol MABr in 1 mL dimethylformamide (DMF): Dimethyl sulfoxide (DMSO) = 9:1 solvent. $MAPbBr_3$ (40 µL) precursor solution was spun coated on ≈1 cm^2 non-porous GaN substrate at 5000 rpm for 60 s. Then the sample was annealed at 100 °C for 10 min to crystallize the $MAPbBr_3$.

Samples for transient characterization were encapsulated in the nitrogen-filled glovebox to reduce perovskite degradation when exposed to air and moisture. A thin glass coverslip was placed on top of the sample, and the sample edges were sealed with epoxy. The sapphire layer was polished off for transient measurements.

$MAPbBr_3$ Thin Film on Quartz Sample Preparation: $MAPbBr_3$ thin film on quartz was prepared with the same method as the $MAPbBr_3$/non-porous sample preparation.

X-Ray Diffraction (XRD): X-ray diffraction was measured with a Bruker X-ray D8 Advanced diffractometer with Cu $K_{\alpha 1,2}$ radiation ($\lambda = 1.541$ Å). The incident beam slit width was 0.6 mm. Data was collected in an angular range 2θ of 5°–55° with an angular resolution of 0.02°.

Scanning Electron Microscopy (SEM): Scanning electron microscopy was conducted on a ZEISS GeminiSEM 300 running at a beam voltage of 2 kV using a probe current of 180–200 pA. Images were taken using an in-column secondary electron detector.

Scanning Transmission Electron Microscopy (STEM): STEM samples were prepared using standard TEM lamella preparation techniques utilizing an FEI Helios focused ion beam (FIB) microscope employing a 30 kV Ga ion source. In brief, on an Au-coated perovskite porous GaN sample, a region of interest was located and Pt-coated to protect the surface from Ga implantation. Two trenches were milled on either side. The lamella was then transferred to a three-posted FIB lift-out grid. The lamella was then thinned to <100 nm using consecutive side milling.

Scanning transmission electron microscopy was conducted in an FEI Osiris running at 200 kV with a beam current of 150 pA and a convergence angle of 24 mrad. STEM BF, ADF, and HAADF imagery were taken simultaneously, and STEM-EDX data was taken using 4 Super-X solid-state X-ray detectors.

Steady-State UV–vis Spectroscopy: Steady-state absorbance of samples was taken with a Shimadzu UV-3600 Plus spectrophotometer, which consists of three detectors: a photomultiplier tube (PMT) for ultraviolet and visible regions, an InGaAs detector and a cooled PbS detector for the near-infrared region. The whole wavelength range covers from 185 to 3300 nm with a maximum resolution of 0.1 nm.

Atomic Force Microscopy Measurements: The thickness of $MAPbBr_3$ thin films on quartz substrates was obtained by atomic force microscopy using a Digital Instruments Dimension 3100 microscope.

Steady-State Photoluminescence Spectroscopy: The steady-state photoluminescence (PL) spectra were measured with the Edinburgh Instruments FLS 980 spectrofluorometer. The spectrometer contains one R928P PMT detector, measuring wavelengths ranging from 200 to 870 nm with a dark count rate smaller than 50 cps at −20 °C. Depending on the samples' emission wavelength, the PL spectra were measured from 450 to 700 nm. Samples were excited at various wavelengths by a 450 W xenon arc lamp depending on the absorbance of samples. The xenon arc light was focused onto a monochromator using an off-axis ellipsoidal mirror.

Photoluminescence Quantum Efficiency (PLQE): Photoluminescence quantum efficiency (PLQE) measurements were taken with the John de Mello method.[44] All samples were excited with a 405 nm continuous-wave (CW) laser at excitation power ≈300 µW, and the emission was collected with an Andoe iDus DU490A Si detector.

Time-Correlated Single-Photon Counting (TCSPC): Samples were excited with a PicoQuant LDH407 laser diode at 407 nm with a repetition rate of 2 MHz at a fluence of 7.37×10^{-2} µJ cm^{-2} per pulse. The emission signal was selected with a monochromator to get the desired wavelength and detected by a Hamamastu R3809U-50 photomultiplier detector. Color filters were utilized to remove the scattered photons from the excitation laser. A neutral density filter was used to ensure that no more than one photon was detected in every photoexcitation cycle.

The TCSPC measurements at 255 nm excitation were performed using an Edinburgh Instruments Life Spec system, FLS1000. The sample was excited with a picosecond pulsed light emitting diode (EPLED-255, Edinburgh Instruments) with a wavelength of 255 nm, 70 nJ cm^{-2} per pulse over the illuminated area. The output signals were recorded using a Princeton Instruments monochromator fiber connected to a low-noise Avalanche Photodiode from Excelitas.

Intensified CCD (ICCD): Samples were excited by a femtosecond laser generated from second harmonic generation (SHG) of a fundamental Ti: sapphire Spectra-Physics Solstice laser source (Wavelength 800 nm, pulse with 80 fs) with a β–barium borate crystal, at a repetition rate of 1 kHz. The excitation laser wavelength was 400 nm. The photoluminescence of samples was detected by an electrically-gated intensified charge-coupled device (ICCD) camera (Andor iStar DH740 CCI-010) and a calibrated grating spectrometer (Andor SR303i). A 425 nm long-pass filter was used to remove the scattered laser signal.

Transient Absorption (TA): The output of a Ti:sapphire amplifier system (Spectra Physics Solstice Ace) operating at 1 kHz and generating ≈100 fs pulses was split into the pump and probe beam paths. The 400 nm pump pulses were created by sending the 800 nm fundamental beam of the Solstice Ace through a second harmonic generating (SHG) beta barium borate (BBO) crystal of 1 mm thickness (Eksma Optics). The visible pump pulses (between 520 and 780 nm) were generated in a home-built non-collinear optical parametric amplifier (NOPA). The 340 nm pump pulses were created by focusing the 700 nm output from the NOPA through a BBO crystal (Eksma Optics). The pump was blocked by a chopper wheel rotating at 500 Hz. The UV–vis broadband beam (330–700 nm) was generated by focusing the 800-nm fundamental beam onto a CaF_2 crystal (Eksma Optics, 5 mm) connected to a digital motion controller (Mercury C-863 DC Motor Controller) after passing through a mechanical delay stage (Thorlabs DDS300-E/M). The transmitted pulses were collected with a monochrome line scan camera (JAI SW-4000M-PMCL, spectrograph: Andor Shamrock SR-163) with collected data fed straight into the computer.

Supporting Information

Supporting Information is available from the Wiley Online Library or from the author.

Acknowledgements

The authors would like to acknowledge the financial support of Royal Society Research Grant RGR2232428. R.A.O would like to acknowledge the financial support of EPSRC under EP/M010589/1 and EP/X017028/1. X.B. and L.D. would like to acknowledge financial support from the Chinese Scholarship Council and the Cambridge Trust. X.B. and M.I.D. acknowledge funding from the Royal Society University Research Fellowship. Martin Frentrup is thanked for his assistance in the interpretation of the XRD data. M.S. would like to acknowledge the financial support of EPSRC under EP/N509620/1 and EP/R513180/1.

Conflict of Interest

The authors declare no conflict of interest.

Author Contributions

X.B. fabricated all the perovskite/GaN samples and performed the XRD characterizations and optical measurements, including absorption, photoluminescence, photoluminescence quantum efficiency, and transient

© 2024 The Author(s). Advanced Optical Materials published by Wiley-VCH GmbH

photoluminescence under the supervision of R.H.F. L.D. carried out the transient absorption measurement under the supervision of N.C.G. S.M.F. prepared focused ion beam milling samples, performed the scanning transmission electron microscopy measurement, and analyzed results. M.S. performed focused ion beam milling-scanning electron microscope and scanning electron microscope measurements. P.H.G. prepared all the GaN samples in this research. A.G. helped with scanning electron microscope measurements. R.A.O. supervised S.M.D., M.S., P.G., and A.G. Y.S. assisted with the sample preparation for focused ion beam milling. R.H.F., R.A.O., and M.I.D. contribute to the discussion of the results. X.B. analyzed the results and drafted the manuscript with contributions from all the other co-authors.

Data Availability Statement

The data that support the findings of this study are available from the corresponding author upon reasonable request.

Keywords

charge carrier dynamics, gallium nitride, nanocrystals, perovskites, porous materials

Received: January 24, 2024
Revised: March 12, 2024
Published online:

[1] X. Zhou, P. Tian, C. W. Sher, J. Wu, H. Liu, R. Liu, H. C. Kuo, *Prog. Quantum Electron.* **2020**, *71*, 100263.
[2] Y. M. Huang, J. H. Chen, Y. H. Liou, K. J. Singh, W. C. Tsai, J. Han, C. J. Lin, T. S. Kao, C. C. Lin, S. C. Chen, H. C. Kuo, *Nanomater* **2021**, *11*, 2696.
[3] M. S. Wong, C. Lee, D. J. Myers, D. Hwang, J. A. Kearns, T. Li, J. S. Speck, S. Nakamura, S. P. Denbaars, *Appl. Phys. Express* **2019**, *12*, 097004.
[4] J.-S. Park, J. K. Kim, J. Cho, T.-Y. Seong, *ECS J. Solid State Sci. Technol.* **2017**, *6*, Q42.
[5] C. Zhang, S. H. Park, D. Chen, D. W. Lin, W. Xiong, H. C. Kuo, C. F. Lin, H. Cao, J. Han, *ACS Photonics* **2015**, *2*, 980.
[6] T. Zhu, Y. Liu, T. Ding, W. Y. Fu, J. Jarman, C. X. Ren, R. V. Kumar, R. A. Oliver, *Sci. Rep.* **2017**, *7*, 1.
[7] K. J. Lee, J. W. Min, B. Turedi, A. Y. Alsalloum, J. H. Min, Y. J. Kim, Y. J. Yoo, S. Oh, N. Cho, R. C. Subedi, S. Mitra, S. E. Yoon, J. H. Kim, K. Park, T. H. Chung, S. H. Jung, J. H. Baek, Y. M. Song, I. S. Roqan, T. K. Ng, B. S. Ooi, O. M. Bakr, *ACS Energy Lett.* **2020**, *5*, 3295.
[8] M. R. Zhang, X. Q. Chen, G. B. Pan, *Sens. Actuators, B* **2017**, *240*, 142.
[9] M. Shafa, D. Priante, R. T. Elafandy, M. N. Hedhili, S. T. Mahmoud, T. K. Ng, B. S. Ooi, A. Najar, *ACS Omega* **2019**, *4*, 1678.
[10] R. Xi, S. H. Zhang, L. Zhang, C. Wang, L. J. Wang, J. H. Yan, G. B. Pan, *Sensors* **2019**, *19*, 606.
[11] K. Sarkar, P. Kumar, *Appl. Surf. Sci.* **2021**, *566*, 150695.
[12] M. R. Zhang, X. Q. Chen, G. B. Pan, *ChemistrySelect* **2016**, *1*, 3159.
[13] Z. Gong, A. Kuehne, A. Kanibolotsky, Y. Chen, I. Perepichka, A. Mackintosh, E. Gu, P. Skabara, R. Pethrick, I. Watson, D. Bradley, G. Heliotis, P. Stavrinou, C. Griffin, C. Jeon, *Opt. Express* **2009**, *17*, 16436.
[14] R. Kumar, S. S. Kushvaha, M. Kumar, M. S. Kumar, G. Gupta, K. Kandpal, P. Kumar, *Sci. Reports* **2020**, *10*, 1.
[15] Y. Weng, G. Chen, J. Nie, S. Que, S.-H. Song, Y. Yu, F. Zhang, H. Liu, X. Zhou, Y. Zhang, J. Sun, J.-K. Song, C. Wu, T. Guo, Q. Yan, *ACS Omega* **2022**, *7*, 5502.
[16] J. H. Kang, B. Li, T. Zhao, M. A. Johar, C. C. Lin, Y. H. Fang, W. H. Kuo, K. L. Liang, S. Hu, S. W. Ryu, J. Han, *ACS Appl. Mater. Interfaces* **2020**, *12*, 30890.
[17] S.-W. H. Chen, Y.-M. Huang, K. J. Singh, Y.-C. Hsu, F.-J. Liou, J. Song, J. Choi, P.-T. Lee, C.-C. Lin, Z. Chen, J. Han, T. Wu, H.-C. Kuo, *Photonics Res.* **2020**, *8*, 630.
[18] Z. Hu, Y. Yin, M. U. Ali, W. Peng, S. Zhang, D. Li, T. Zou, Y. Li, S. Jiao, S. J. Chen, C. Y. Lee, H. Meng, H. Zhou, *Nanoscale* **2020**, *12*, 2103.
[19] M. A. Green, A. Ho-Baillie, H. J. Snaith, *Nat. Photonics* **2014**, *8*, 506.
[20] M. V. Kovalenko, L. Protesescu, M. I. Bodnarchuk, *Science* **2017**, *358*, 745.
[21] K. Miyata, D. Meggiolaro, M. T Trinh, P. P. Joshi, E. Mosconi, S. C. Jones, F. De Angelis, X. Y. Zhu, *Sci. Adv.* **2017**, *3*.
[22] E. R. Dohner, A. Jaffe, L. R. Bradshaw, H. I. Karunadasa, *J. Am. Chem. Soc.* **2014**, *136*, 13154.
[23] Z. K. Tan, R. S. Moghaddam, M. L. Lai, P. Docampo, R. Higler, F. Deschler, M. Price, A. Sadhanala, L. M. Pazos, D. Credgington, F. Hanusch, T. Bein, H. J. Snaith, R. H. Friend, *Nat. Nanotechnol.* **2014**, *9*, 687.
[24] H. Cho, S.-H. Jeong, M.-H. Park, Y.-H. Kim, C. Wolf, C.-L. Lee, J. H. Heo, A. Sadhanala, N. Myoung, S. Yoo, S. H. Im, R. H. Friend, T.-W. Lee, *Science* **2015**, *350*, 1222.
[25] F. Zhang, H. Zhong, C. Chen, X. Wu, X. Hu, H. Huang, J. Han, B. Zou, Y. Dong, *ACS Nano* **2015**, *9*, 4533.
[26] J. S. Manser, M. I. Saidaminov, J. A. Christians, O. M. Bakr, P. V. Kamat, *Acc. Chem. Res.* **2016**, *49*, 330.
[27] J. M. Richter, M. Abdi-Jalebi, A. Sadhanala, M. Tabachnyk, J. P. H. Rivett, L. M. Pazos-Outón, K. C. Gödel, M. Price, F. Deschler, R. H. Friend, *Nat. Commun.* **2016**, *7*, 13941.
[28] B. Wenger, P. K. Nayak, X. Wen, S V Kesava, N. K. Noel, H. J. Snaith, *Nat. Commun.* **2017**, *8*, 590.
[29] N. Droseros, G. Longo, J. C. Brauer, M. Sessolo, H. J. Bolink, N. Banerji, *ACS Energy Lett.* **2018**, *3*, 1458.
[30] L. M. Falk, K. P. Goetz, V. Lami, Q. An, P. Fassl, J. Herkel, F. Thome, A. D. Taylor, F. Paulus, Y. Vaynzof, *Energy Technol.* **2020**, *8*, 1900737.
[31] D. N. Dirin, L. Protesescu, D. Trummer, I. V. Kochetygov, S. Yakunin, F. Krumeich, N. P. Stadie, M. V. Kovalenko, *Nano Lett.* **2016**, *16*, 5866.
[32] A. Loiudice, S. Saris, E. Oveisi, D. T. L. Alexander, R. Buonsanti, *Angew. Chem., Int. Ed.* **2017**, *56*, 10696.
[33] S. Demchyshyn, J. M. Roemer, H. Groiß, H. Heilbrunner, C. Ulbricht, D. Apaydin, A. Böhm, U. Rütt, F. Bertram, G. Hesser, M. C. Scharber, N. S. Sariciftci, B. Nickel, S. Bauer, E. D. Głowacki, M. Kaltenbrunner, *Sci. Adv.* **2017**, *3*, e1700738.
[34] J. Burschka, N. Pellet, S. J. Moon, R. Humphry-Baker, P. Gao, M. K. Nazeeruddin, M. Grätzel, *Nature* **2013**, *499*, 316.
[35] K. T. P. Lim, C. Deakin, B. Ding, X. Bai, P. Griffin, T. Zhu, R. A. Oliver, D. Credgington, *APL Mater.* **2019**, *7*, 021107.
[36] K. H. Wang, L. C. Li, M. Shellaiah, K. W. Sun, *Sci. Reports* **2017**, *7*, 1.
[37] H. Shen, R. Nan, Z. Jian, X. Li, *J. Mater. Sci.* **2019**, *54*, 11596.
[38] D. F. Swinehart, *J. Chem. Educ.* **1962**, *39*, 333.
[39] Y. Calahorra, B. Spiridon, A. Wineman, T. Busolo, P. Griffin, P. K. Szewczyk, T. Zhu, Q. Jing, R. Oliver, S. Kar-Narayan, *Appl. Mater. Today* **2020**, *21*, 100858.
[40] J. Gong, S. Liu, Y. He, X. Feng, X. Xia, Z. Quan, L. Wang, *Appl. Phys. Lett.* **2017**, *111*, 122103.
[41] M. A. Reshchikov, J. D. McNamara, H. Helava, A. Usikov, Y. Makarov, *Sci. Reports* **2018**, *8*, 1.
[42] M. Julkarnain, N. Kamata, T. Fukuda, Y. Arakawa, *Opt. Mater.* **2016**, *60*, 481.
[43] Q. Wang, X.-D. Liu, Y.-H. Qiu, K. Chen, L. Zhou, Q.-Q. Wang, *AIP Adv.* **2018**, *8*, 25108.
[44] J. C. De Mello, H. F. Wittmann, R. H. Friend, *Adv. Mater.* **1997**, *9*, 230.
[45] T. L. Schmidt, K. Lischka, W. Zulehner, *Phys. Rev. B* **1992**, *45*, 8989.

© 2024 The Author(s). Advanced Optical Materials published by Wiley-VCH GmbH